Scientific Research Publishing

Modern Mechanical Engineering, 2023, 13, 77-100
https://www.scirp.org/journal/mme
ISSN Online: 2164-0181
ISSN Print: 2164-0165

Critical Assessment of Slope Stability: A Case Study on the Toffo-Lalo Road Project

Guy Oyéniran Adeoti[1], Judicaël Koffi Agbelele[1,2], Crespin Prudence Yabi[1], Rufin Nongnidé Kinhoun[1], Éric Adéchina Alamou[1]

[1]Laboratory of Testing and Studies in Civil Engineering (L2EGC), National University of Science, Technology, Engineering, and Mathematics (UNSTIM), Abomey, Benin
[2]National School of Technical Education (ENSET), Lokossa, Republic of Benin
Email: adeotiguy@unstim.bj

How to cite this paper: Adeoti, G.O., Agbelele, J.K., Yabi, C.P., Kinhoun, R.N. and Alamou, É.A. (2023) Critical Assessment of Slope Stability: A Case Study on the Toffo-Lalo Road Project. *Modern Mechanical Engineering*, **13**, 77-100.
https://doi.org/10.4236/mme.2023.134006

Received: April 1, 2023
Accepted: November 11, 2023
Published: November 14, 2023

Abstract

This article systematically delves into a comprehensive analysis of the latest and most advanced techniques for the assessment of slope stability. It particularly focuses on strategies aimed at enhancing slope stability in road construction. In addition to this analysis, the article presents an illustrative case study centered on the Toffo-Lalo Road Project. The core objective of this paper is to scrutinize the stability of large embankments in road construction, with a specific emphasis on the development and asphalt overlay of the Toffo-Lalo road. This scrutiny is conducted through the utilization of stability calculation software, GEOSTUDIO2018, specifically its SLOPE/W module. Within this framework, a detailed model of the cutbank located at KP1+750-2+250 was meticulously developed. This model takes into account the physical-mechanical characteristics of the soil at the site, as well as the topographic layout. Its attributes include a cohesion value of 11.3 Kpa, a density of 16.57 KN/m^3, and a friction angle of 27˚. The modeling results, employing the Morgenstern-Price method—an approach renowned for its adherence to equilibrium conditions and provision of precise results—conclude that the safety coefficient (*Fs* = 1.429) prior to any reinforcement signifies a critical state of slope stability. To address this, the article explores the implementation of reinforcement techniques, particularly focusing on rigid inclusions like nailing and piles. The modeling exercises reveal a noteworthy enhancement in the safety coefficient (*Fs*) post-reinforcement. Furthermore, the article undertakes a parametric study to optimize the reinforcement strategies. This analysis highlights that anchoring at 0˚ downward relative to the horizontal plane and employing a pile angle of 90˚ represent the most favorable approaches. These measures yield safety coefficients of 3.60 and 2.34, respectively, indicating substantially improved slope stability.

Keywords

GEOSLOPE, Morgenstern-Price Method, Numerical Modelling, Safety Coefficient, Soil Cohesion and Slope Stability

1. Introduction

Slope movements, with their blend of drama and, on occasion, tragedy, have long been a cause for concern. In certain regions, they rank as a primary driver of human and economic losses. The reasons behind the instability of both natural and man-made slopes are as diverse as the landscapes they affect. The creeping or sudden shifts of natural slopes can wreak havoc on infrastructure and buildings, inflicting substantial economic costs and, regrettably, human casualties. Benin, amidst its extensive infrastructure development endeavors, grapples continuously with this phenomenon.

In the pages of documented history and within the PASEK records, we find accounts of ground movements that have led to approximately 150,000 casualties. Among these historical events, the Mont Granier collapse stands out prominently. This devastating event, which unfolded north of Chambéry in November 1248, is estimated to have claimed between 1500 and 5000 lives (GOGUEL-PACHOUD 1972). More recent in memory are the instances of mudslides that have resulted in the tragic loss of human lives. Notably, the Roquebillières incident in the Alpes Maritimes in 1926 claimed 17 lives, while the Sanatorium du Plateau d'Assy tragedy in 1970 took the lives of 43 individuals.

The stability of slopes is a pressing concern for geotechnicians, encompassing both practitioners and researchers alike. Investigating the stability of a slope involves a multifaceted approach, including site evaluation and the selection of soil mechanical properties, culminating in comprehensive stability calculations. These calculations serve a dual purpose: identifying the critical failure surface, where the risk of a landslide is most acute, and determining the corresponding safety coefficient. Numerous methodologies have emerged to address these landslide-related challenges [1] [2] [3] [4]. Among these, classical limit equilibrium methods and Discontinuous Methods, particularly the Discrete Element Method (DEM) [4] [5] [6] [7] [8], are prominent.

Given the gravity of these challenges, our efforts have been dedicated to a comprehensive numerical analysis aimed at addressing the stability concerns related to the Toffo-Lalo route. Our objectives encompassed:

- The utilization of the GEOSTUDIO2018 calculation tool to evaluate the stability of the embankment slope along the Toffo-Lalo route, spanning from PK1+750 to PK2+250;
- The simulation of various reinforcement methods for the embankment slope in this specific section of the Toffo-Lalo route;
- The execution of a parametric study aimed at optimizing the selected rein-

forcement solutions for the embankment slope;

- The successful completion of stability calculations for the embankment slope using the GEOSTUDIO2018 tool within the PK1+750 to PK2+250 section of the Toffo-Lalo route;
- The implementation of simulations to assess different reinforcement methods for the embankment slope in this particular segment;
- The accomplishment of a thorough parametric study to enhance and optimize the chosen reinforcement solutions.

The primary aim of this study is to conduct a comprehensive analysis of cutting-edge techniques employed in the management of unstable terrains and to explore strategies for enhancing slope stability. In addition, this article features an illustrative case study centered around the Toffo-Lalo Road Project.

1.1. Exploring Modern Approaches to Stability Analysis

Stability analysis of a slope, whether it pertains to natural terrain or an artificial embankment, aims to address two fundamental questions:

- What is the likelihood of a landslide occurrence?
- If a landslide does occur, what is the geometry of the failure surface?

The answers to these questions, based on the specific context, are crucial in identifying potential sliding scenarios and deriving conclusions to ensure the safety of both individuals and structures. Conducting stability analyses for embankments presents a complex challenge due to the multitude of influencing factors, including topography, hydraulic conditions, human activities (such as construction projects or dam drainage), and geological characteristics. Additionally, the mechanical properties of soils often exhibit heterogeneity, anisotropy, and discontinuities. Generally, three primary types of instabilities are recognized: slides involving distinct failure surfaces (often circular in shape), mudflows, and rockfalls. For the scope of this study, we will focus solely on the first type of instability.

1.1.1. Safety Factor

A safety factor, denoted as F, serves as an indicator of the risk associated with potential slope failure. It is influenced by the selected calculation method, the stress state within the slope, the properties of the medium, and the geometry of the failure surface. Two distinct definitions are commonly used [9] [10].

According to the first definition, the safety factor is the value by which the soil's strength must be divided to initiate a failure. This factor is represented as F_1. This definition is widely adopted and is utilized in equilibrium-based methods, as well as in the subsequently described SSRM and GIM methods.

The second, more physically grounded definition, characterizes the safety factor as the ratio between resisting forces and driving forces (Equation (1)), denoted as F_2.

$$F_2 = \frac{\int_s \tau_{rupt} \mathrm{d}s}{\int_s \tau \mathrm{d}s} \tag{1}$$

In theory, if F is less than 1, the slope is considered unstable. Conversely, if F is greater than 1, the slope is deemed stable. In practical terms, to account for uncertainties stemming from calculations or the determination of site characteristics, a safety factor is introduced according to Duncan (1996) [11]. Broadly, the following guidelines are followed:

- If $F<1$, there is a hazard;
- If $1 \le F<1.25$, safety is subject to question;
- If $1.25 \le F<1.4$, safety might be judged acceptable if the potential consequences of a slope failure are minimal;
- If $F \ge 1.4$, safety is considered satisfactory.

The specified ranges of values can be adjusted depending on the potential impact of a slope failure.

1.1.2. Determination of Critical Failure Surface, 2D or 3D Analysis

The systematic quest for the critical failure surface entails, in its initial phase, delineating a set of potential failure surfaces: one might opt, for instance, to confine consideration to planar or circular failure surfaces (this selection should be informed by on-site observations). Subsequently, the safety factor is computed for each of these surfaces. The critical failure surface is the one linked to the smallest safety factor. This straightforward technique yields satisfactory outcomes in the majority of cases; however, it necessitates testing a considerable number of failure surfaces, a process that can be laborious. Moreover, it mandates restricting the analysis to geometrically uncomplicated failure surfaces.

Due to these considerations, algorithms designed to identify critical failure surfaces have been introduced, and these include contributions by Baker (1980), Celestino & Duncan (1981), Greco & Gulla (1985), Nguyen (1985), Li & White (1987), Chen (1992), Greco (1996), Hussein *et al.* (2001), and Cheng (2003), among others [12]-[20].

Presently, most stability assessments are conducted within a 2D framework; however, as computational capabilities continue to advance, the adoption of a three-dimensional approach is progressively gaining traction. Generally, safety factors calculated in 2D are marginally lower than those computed in 3D, as 2D analysis focuses on the cross-section of a slope that is the least stable.

1.2. Key Limit Equilibrium Methods

Currently, limit equilibrium methods remain the most widely employed techniques for conducting stability analyses. These methods involve partitioning the soil into sufficiently narrow slices such that their bases can be approximated as straight segments. The next step is to formulate equilibrium equations for forces and/or moments. Various adaptations have emerged based on the assumptions about forces between slices and the chosen equilibrium equations (**Table 1**). These adaptations typically yield reasonably consistent outcomes, with discrepancies in computed F values often remaining below 6%, as reported by Duncan (1996) [11].

Table 1. Key limit equilibrium methods.

Methods	Advantages and Disadvantages
Ordinary Method of Slices (Fellenius, 1927) [21]	- Circular surfaces only - Satisfies moment equilibrium
Bishop's Modified Method (Bishop, 1955) [22]	- Circular surfaces only - Satisfies moment equilibrium - Satisfies vertical force equilibrium but not horizontal force equilibrium
Force Equilibrium Method (Lowe & Karafiath, 1960; US Army Corps of Engineers, 1970) [23] [24]	- Suitable for all rupture surface geometries - Does not satisfy moment equilibrium - Satisfies vertical and horizontal force equilibrium
Morgenstern & Price's Method (Morgenstern & Price, 1965) [25]	- More frequent numerical instability compared to other methods - Suitable for all rupture surface geometries - Satisfies all equilibrium conditions
Spencer's Method (Spencer, 1967) [26]	- Suitable for all rupture surface geometries - Satisfies all equilibrium conditions
Janbu's Generalized Procedure of Slices (Janbu, 1968) [27]	- Suitable for all rupture surface geometries - Satisfies all equilibrium conditions
Slope Stability Charts (Janbu, 1968; Duncan, 1987) [27] [28]	- Satisfactory results in many cases - Quick computation

1.2.1. Fellenius' Method (1927)

The benchmark limit equilibrium methods are the formulations proposed by Fellenius (1927) [21] and Bishop (1955) [22]. **Figure 1** illustrates the division of a potentially unstable slope. The horizontal equilibrium for slice i can be expressed as (Equation (2)):

$$dH_i - \sigma_i \tan\alpha_i dx + \tau_i dx = 0 \tag{2}$$

Here, H_i represents the horizontal force component between two slices, σ_i and τ_i denote the normal and tangential stresses on the potential failure surface at the level of slice i and α_i signifies the angle formed between the base of slice i and the horizontal (**Figure 1**).

The vertical equilibrium for slice i can be described by (Equation (3)):

$$dV_i - \gamma_i h_i dx + \sigma_i dx + \tau_i \tan\alpha_i dx = 0 \tag{3}$$

In this equation, V_i indicates the vertical force component between two slices, and γ_i represents the weight of slice i.

In Fellenius's method (1927), an assumption is made that both dH_i and dV_i are equal to zero, leading to the estimation of normal stresses using (Equation (4)):

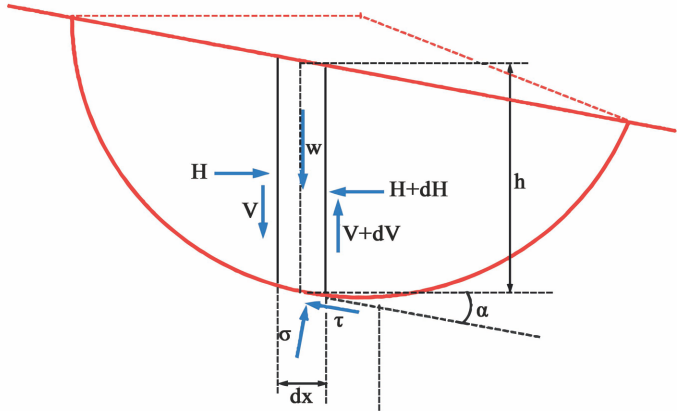

Figure 1. Circular failure analysis using bishop and fellenius approaches.

$$\sigma_i = \gamma h_i \cos^2 \alpha_i \tag{4}$$

By utilizing the global definition of the safety factor, Equation (5) is obtained.

$$F_{Fel} = \frac{\sum_{i=1}^{n}\left(C' + \left(\gamma h_i \cos^2 \alpha_i - u_i\right)\tan\varphi'\right)\frac{1}{\cos\alpha_i}}{\sum_{i=1}^{n}\gamma h_i \sin\alpha_i} \tag{5}$$

1.2.2. Bishop's Method (1955)

In Bishop's method (1955), the assumption $dV_i = 0$ is employed. By considering the global definition of the safety factor, is derived: $\sigma_i = \gamma_i h_i - \tau_i\left(F_{Bish}\right)\tan\alpha_i$ This yields a relationship of the form: $F_{Bish} = f\left(F_{Bish}\right)$ (Equation (6)). The safety factor is determined using an iterative process known as the fixed-point method. For instance, Alexis (1987) [29] applied this method to study the stability of sediment ponds and channels in the Lorient harbor.

$$F_{Bish} = \frac{\sum_{i=1}^{n}\left(C' + \left(\gamma h_i - \left(\frac{C'}{F_{Bish}} + \sigma' \frac{\tan\varphi'}{F_{Bish}}\right)\tan\alpha_i - u_i\right)\tan\varphi'\right)\frac{1}{\cos\alpha_i}}{\sum_{i=1}^{n}\gamma h_i \sin\alpha_i} \tag{6}$$

In certain slope scenarios, failure can occur approximately parallel to the slope surface. The calculation model utilized assumes an infinite soil with the water table parallel to the slope surface (see **Figure 2**). Considering the assumption of an infinite slope, the vertical forces exerted on the block's sides can be considered negligible ($V = 0$). Assuming equilibrium of horizontal forces and pressures on each side of the block and stipulating the sum of applied forces is zero, the normal and tangential reactions at the base of the block can be calculated. Thus, employing the Mohr-Coulomb criterion and accounting for long-term drained behavior, the expression for the safety factor can be deduced as follows (Equation (7)):

$$F = \frac{2}{\sin(2\alpha)}\frac{C'}{g\rho} + \frac{\left(\rho h - \rho_w h_w\right)\tan\varphi'}{\rho h \tan\alpha} \tag{7}$$

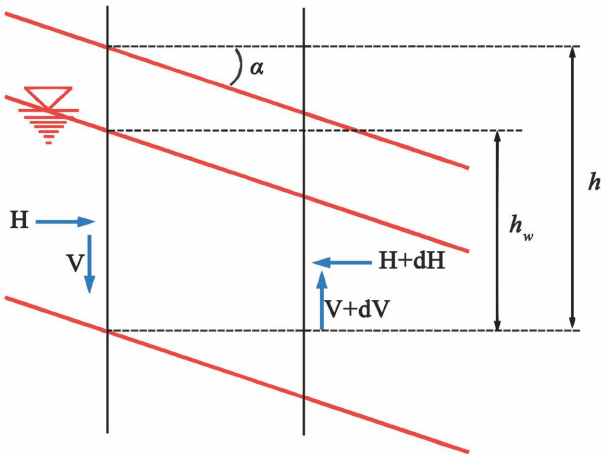

Figure 2. Failure plane.

Two primary factors contribute to the prevalence of limit equilibrium methods:

- They are straightforward, familiar, and comprehensible to all stakeholders in the field;
- They rely on a limited set of parameters, avoiding the need to parameterize soil behavior laws, for instance.

However, these methods do have significant limitations. They do not incorporate soil behavior, struggle to accurately address complex scenarios (such as construction stages, dynamic loads, hydro-mechanical coupling, etc.), and assume constant safety factors along the failure surface (utilizing the global definition of the safety factor F_1).

2. Materials and Methods

2.1. Study Area Description

The focus of the present investigation lies within the PK1+750 to PK2+250 section, which holds a distinctive character due to its traversal of regions abundant in agricultural potential but bereft of proper road infrastructure. Specifically, the route extending from Lalo to Toffo serves as an extension of an existing unpaved road, plagued by poor accessibility, particularly during the rainy season when it succumbs to inundation from the Couffo River valley and the Tchi median depression. This geographical expanse is distinguished by the presence of numerous water bodies, most notably the Mono-Couffo basin. This basin encompasses the Couffo River, which stretches for 190 km, with 170 km of its course winding through Benin before ultimately flowing into Lake Ahémé, covering an area of 78 km^2 before making its journey to the Atlantic Ocean. The topography of the region is characterized by gentle undulations and predominantly consists of a silico-clay plateau. Vegetation in the study area showcases remarkable diversity, including savannah with species like orange and palm trees, alongside a designated forested area known as "La Lama" (**Figure 3** & **Figure 4**).

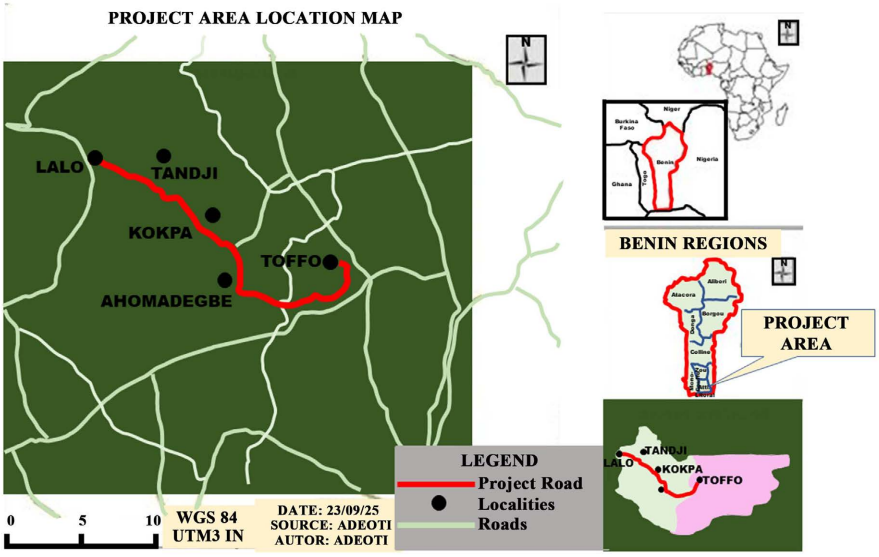

Figure 3. Study area location map.

Figure 4. Slope instabilities in the study area.

2.2. Geotechnical Analysis of the Study Site

Geotechnical assessments are indispensable for providing an accurate depiction of terrains and estimating their physical and mechanical properties, which play a vital role in subsequent calculations. Typically, two primary categories of geotechnical assessments exist: in-situ tests and laboratory experiments.

The conducted geotechnical survey involved the placement and execution of two boreholes. Its primary objective was to enhance our understanding of the lithological composition and the physical and mechanical characteristics of the soils in their natural state. A core drilling survey was conducted at the Toffo-Lalo site at PK1+750, PK2+000, and PK2+250.

The interpretation of the core drilling survey results is as follows:

- Borehole SC 01:

  0 - 10 meters: Loamy gravelly clay, lightly compacted, with a brown coloration.

- Borehole SC 02:
  0 - 10 meters: Loamy gravelly clay, lightly compacted, with a brown coloration.
- Borehole SC 03:
  0 - 10 meters: Loamy gravelly clay, lightly compacted, with a brown coloration.

Laboratory tests encompass both physical and mechanical assessments. Notable examples include grain size analysis, Atterberg limits determination, and the direct shear test within a rectangular container. The outcomes of these examinations are presented in the subsequent tables and graphs.

Table 2 (Physical Test Results) presents a comprehensive overview of critical geotechnical test results, including particle size analysis and Atterberg limit tests conducted on soil samples obtained from different boreholes and sides. The borehole locations where soil samples were collected are KP1+750, KP2+200, and KP2+250, corresponding to the Left, Axis, and Right positions from which each soil sample was taken.

Particle Size Analysis:

- All samples exhibit a maximum particle size Dmax of less than 50 millimeters, indicating that the largest particles in the samples are smaller than 50 mm. This suggests that the soil in each borehole contains no particles larger than 50 millimeters, a critical characteristic for understanding soil coarseness or fineness.
- The percentage of soil particles that can pass through a sieve with a nominal size of 0.080 millimeters varies between 38% and 48%. For instance, at KP1+750, where 44% of particles pass through a 0.080 mm sieve, we can infer that the soil contains a significant proportion of fine particles. Conversely, the sample at KP2+200 exhibits a slightly higher fine particle content (48%).

Atterberg Limit Tests:

- Liquid limit (WL) is a crucial parameter indicating the moisture content at which the soil transitions from a liquid to a plastic state. The relatively consistent liquid limit values of 38 across all samples at KP1+750, KP2+200, and KP2+250 suggest a consistent behavior within the soil.
- Plastic limit (WP) represents the moisture content at which the soil starts exhibiting plastic behavior. While there is some variation in plastic limit values (ranging from 21 to 23), all samples fall within a similar range, indicating a comparable plasticity threshold.
- Plasticity index (IP) is the range of moisture content over which the soil behaves in a plastic state. Calculated as the difference between the liquid limit (WL) and plastic limit (WP), IP provides insights into the soil's plasticity. In this dataset, IP values range from 15 to 17, indicating moderate to slightly high plasticity.

Interpretation:

Table 2 highlights essential characteristics of the tested soil samples. Uniform "D_{max}" values indicate a lack of coarse-grained materials in all samples, suggesting that these soils are not predominantly composed of larger particles. Differences in the percentage of particles passing through the 0.080 mm sieve indicate

Table 2. Physical test results.

Borehole (KP)	Side	Particle Size Analysis		Atterberg Limit		
		D_{max}	Passing %0.080 mm	WL	WP	IP
1+750	Left	<50 mm	44%	38	23	15
2+200	Axis	<50 mm	48%	38	21	17
2+250	Right	<50 mm	38%	38	22	16

varying fine-grained content among the samples. The consistent liquid limit values suggest that the soils have similar moisture thresholds for transitioning from a liquid to a plastic state. Slight variations in plastic limit values are within an acceptable range, indicating similar plastic behavior. The plasticity index values indicate moderate to slightly high plasticity, which can influence soil behavior and compaction.

These results are instrumental in geotechnical engineering, aiding in soil characterization for various applications, such as foundation design, slope stability assessment, and construction material selection. Understanding the soil's physical properties is fundamental to ensuring the success and safety of geotechnical projects, which are founded on sound geotechnical principles.

Referring to the soil classification criteria defined in the NF P 11-300 standard (**Figure 5**), the on-site soil is unequivocally classified as Class A, denoting "fine soils". This classification is based on a comprehensive analysis of soil samples extracted from drilling operations conducted at specific locations, namely KP1+750, KP2+00, and KP2+250.

The classification is grounded on two pivotal factors. Firstly, the computed average percentage of particles passing through a sieve with a size of 0.080 millimeters in these drilling samples consistently exceeds the prescribed threshold of 35%. Secondly, the maximum particle size (D_{max}) recorded in these samples consistently remains below 50 millimeters. These criteria align with the defining characteristics of Class A soils, indicating a predominant presence of fine-grained particles.

Furthermore, the outcomes of Atterberg limit tests performed on the same soil unequivocally validate its classification as Class A, more precisely, Class A2*, which specifically categorizes it as "fine clayey sands". This classification is substantiated by the plasticity index (PI) falling within the defined range of 12% to 25% ($12 < PI < 25$), attesting to the soil's distinct plasticity traits.

In essence, in strict accordance with the NF P 11-300 standards, the soil is confidently classified as Class A2*, a classification substantiated both by particle size analysis and Atterberg limit tests. This classification underscores its identity as "fine soils" with discernible clayey sand properties.

Table 3 (Mechanical Test Results) provides data from borehole or well SC01 at different depths intervals of 2.00/2.30 meters, 4.00/4.30 meters, and 6.00/6.30 meters. These depth intervals allow for a comprehensive understanding of the

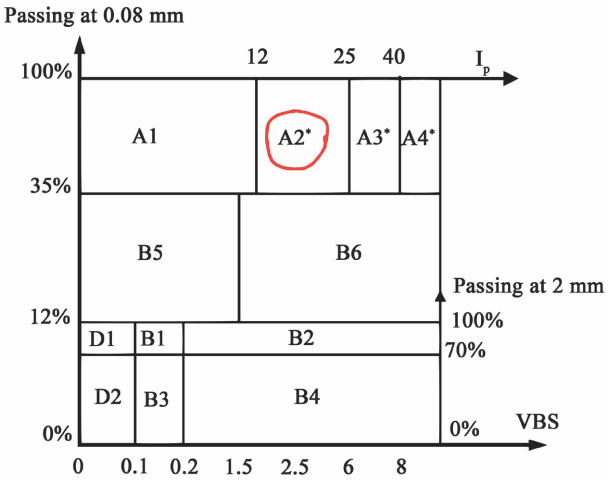

Figure 5. Summary table of soil classification according to their nature (GTR).

Table 3. Mechanical test results.

Borehole/Well	SC01 (KP2+000)		
2 - 4 Depth (m)	2.00/2.30	4.00/4.30	6.00/6.30
Initial Water Content W (%)	7.31	7.30	8.23
Saturation Water Content Ws (%)	23.00	23.00	23.00
Degree of Saturation Sr (%)	32.00	32.00	32.00
Wet Density γ_h (KN/m^3)	17.79	17.79	17.97
Dry Density γ_d (KN/m^3)	16.58	16.58	16.56
Shear Cohesion C_U (Kpa)	10.40	11.30	11.30
Friction Angle φ_u (Degrees)	27.10	27.10	27.10

soil's behavior at varying depths. Table 3 also includes various parameters related to soil mechanics and properties.

Initial Water Content W (%):

Initial water content, expressed as a percentage, signifies the proportion of water present in the soil sample at the outset of testing. Across varying depths, the data indicates that the initial water content ranges from 7.31% to 8.23%. The variations in initial water content (ranging from 7.31% to 8.23%) indicate slight fluctuations in soil moisture levels at different depths. This knowledge is pivotal for construction projects, as it impacts compaction efforts, soil stability, and foundation design. Higher moisture content can affect soil strength and compaction characteristics.

Saturation Water Content Ws (%):

Saturation water content designates the percentage of water content in the soil when it is entirely saturated, meaning it has absorbed the maximum amount of water it can hold. The data shows a consistent saturation water content of 23% at all depths during testing, signifying that the soil reached full saturation. This da-

ta is essential for assessing the soil's hydraulic conductivity and potential for retaining water, which can be vital for projects involving groundwater flow or retaining structures.

Degree of Saturation Sr (%):

The degree of saturation represents the ratio of actual water content to saturation water content, expressed as a percentage. Remarkably, the degree of saturation is uniform at 32% across all depths. This consistency implies that the soil is consistently partially saturated during testing. This knowledge is valuable for understanding how much water the soil can absorb or release, which can affect groundwater interactions and soil behavior in response to changes in moisture levels.

Wet Density γ_h (KN/m^3) and Dry Density γ_d (KN/m^3):

Wet density reflects the density of the soil when it is saturated with water. The dataset portrays wet densities ranging from 17.79 KN/m^3 to 17.97 KN/m^3 at various depths. These values denote the weight and compactness of the soil when fully saturated. Dry density signifies the soil's density when completely devoid of water content. The provided data illustrates a marginal variation in dry density, oscillating between 16.56 KN/m^3 and 16.58 KN/m^3. These figures reveal the soil's compaction characteristics in its dry state.

The variations in wet and dry densities provide insights into the soil's compaction characteristics. The small fluctuations observed suggest relatively consistent compaction levels at different depths. This information is crucial for engineering projects that require specified levels of soil compaction, such as road construction or building foundations.

Shear Cohesion C_U (Kpa) and Friction Angle φ_u (Degrees):

Shear cohesion (C_U) gauges the soil's ability to resist shearing forces when subjected to stress. The dataset shows shear cohesion values ranging from 10.40 Kpa to 11.30 Kpa at different depths. These figures serve as indicators of the soil's strength against shear deformation. The friction angle (φ_u) defines the angle at which soil particles can resist sliding along a surface. Interestingly, the friction angle remains consistent at 27.10 degrees for all depths. This parameter characterizes the soil's internal friction and its capacity to withstand external forces.

The nearly constant values of shear cohesion, ranging from 10.40 Kpa to 11.30 Kpa, and friction angle (consistent at 27.10 degrees) highlight the soil's stable shear strength properties. This is particularly significant for geotechnical engineering projects involving slope stability analysis, excavation, or retaining walls, where understanding shear strength is critical.

Figure 6 and Figure 7 display the resulting Stress Strain Curve and Intrinsic Curve from the test.

Interpretation and Implications:

The data suggests that the soil in borehole SC01 maintains relatively uniform levels of saturation and degree of saturation across the examined depths, offering valuable information for the planning and execution of this study . Both wet and

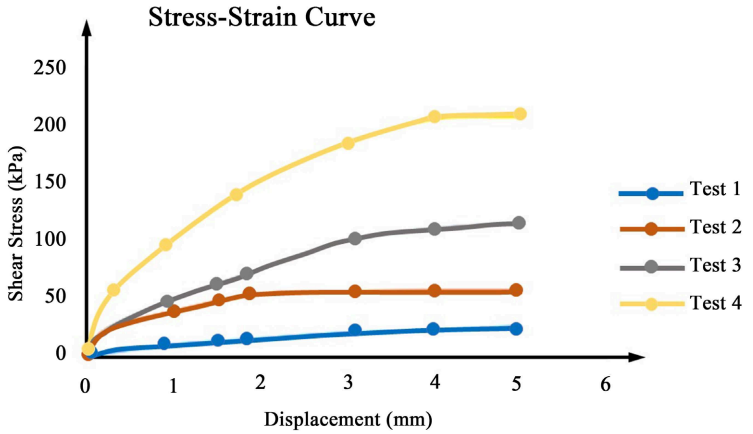

Figure 6. Stress strain curve.

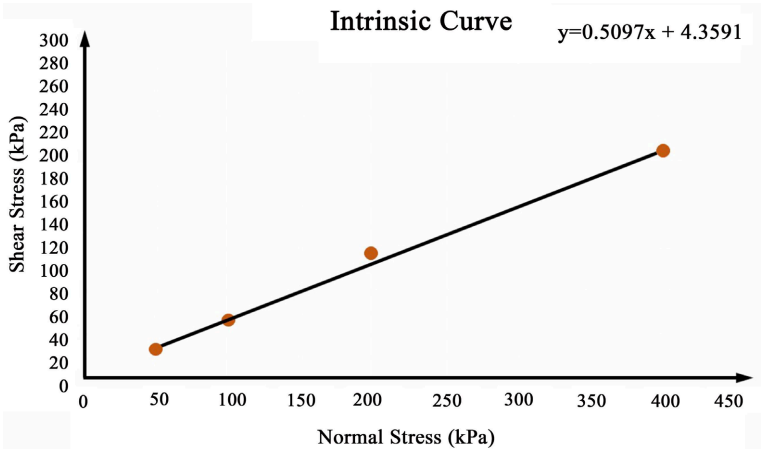

Figure 7. Intrinsic curve.

dry densities exhibit minor fluctuations with depth, indicating a consistent pattern of soil compaction. The moisture content data aids in making decisions regarding soil compaction and construction processes. Understanding the soil's hydraulic properties and compaction behavior can help optimize construction techniques and ensure stable foundations. The nearly constant values of shear cohesion and friction angle signify a stable and uniform shear strength profile throughout the soil at different depths. The shear strength properties are crucial for assessing slope stability, foundation bearing capacity, and overall project safety.

These findings hold significant implications for geotechnical engineering applications, including foundation design and slope stability assessment. The data provides invaluable insights into the mechanical properties and behavior of the soil at varying depths, facilitating informed decision-making in construction and civil engineering projects. This enhanced interpretation offers a comprehensive understanding of the geotechnical test results, highlighting their importance and relevance for engineering assessments and project planning. Consistency in soil properties across depths implies that design and construction strategies can re-

main relatively uniform, simplifying project planning.

In summary, these geotechnical test results provide a solid foundation for making informed decisions in your project or study. They offer insights into soil behavior, strength characteristics, and compaction properties, all of which are vital for successful geotechnical engineering projects.

2.3. Stability Calculation and Reinforcement

The principal aim of this embankment modeling is to evaluate its stability under two conditions: without any reinforcement and when incorporating reinforcement measures.

The software used for calculations in this study adheres to geotechnical calculation principles and has a proven track record of reliability. In 2009, Khebizi Mourad and Guenfoud Mohamed [1] [7] [30] [31] demonstrated the software's efficiency during their numerical modeling of landslides in Constantine's Ciloc city. Geostudio2018 is a comprehensive geotechnical analysis software capable of addressing various soil-related issues such as landslides, settlement, water infiltration in dam structures, and other geotechnical challenges. The software offers multiple integrated programs or modules accessible through its interface, including SEEP/W (for stress-strain relationship analysis), SIGMA/W (for seismic soil behavior analysis), QUAKE/W (for earthquake-induced soil behavior analysis), TEMP/W (for geotechnical soil problem analysis), and SLOPE/W. Of particular interest in this study is SLOPE/W, which facilitates the calculation of safety factors for both natural and engineered slopes. Within SLOPE/W, various methods for computing the safety factor are available, including the Fellenius, Morgenstern-Price, Jumbo, and simplified Bishop methods [1] [4] [31].

Table 4 outlines Software Input Data and Results.

Once the geometric model of the slope is established within the GEO-SLOP calculation code, we proceed to integrate essential components to determine the factors of safety for the slope and the adjacent area. These components encompass soil properties, including soil type, soil model, unit weight, cohesion, and angle of friction, as well as considerations related to the water table or piezometric line.

The geotechnical characteristics of the layer composing the embankment, obtained through experimental analysis, are detailed in **Table 5**.

2.3.1. Geometric Model and Slope Modelling in GEO-SLOP

To create the geometric model of the embankment, we employed the standard cross-sectional and longitudinal profiles applied between KP1+750 and KP2+250. This geometry is represented in a plane deformation model, with dimensions of 20 meters horizontally and 10 meters vertically. The vertical dimension is defined by eight specific points, as outlined in **Table 6**. **Figure 8** illustrates the resulting geometry model within the software.

The applied overload considered for analysis is 1 kilonewton (1 kN), which corresponds to the dead weight of a pedestrian weighing 100 kilograms walking 1 meter from the edge of the embankment on the riverside.

Table 4. Software input data and results.

Software Input Data	Software Results
• Calculation method	• Safety factor
• Geotechnical parameters of the layer: γ, C, and ϕ (degrees)	• Rupture circles
• Slope geometry	• Stresses on slices
• Grid of rupture centers	• Shear strength along the slope length
• Groundwater table level	• Interstitial pressure along the slope

Table 5. Soil properties.

Layer	Color	Bulk Density (KN/m^3)	Cohesion (Kpa)	Friction Angle
Clay	Brown	16.57	11.3	27

Table 6. Coordinates of the slope geometry model.

Item No.	X (m)	Y (m)
1	0	0
2	0	9.5
3	5.5	9.5
4	6.5	9
5	9.5	9
6	15.5	3
7	18	3
8	18	0

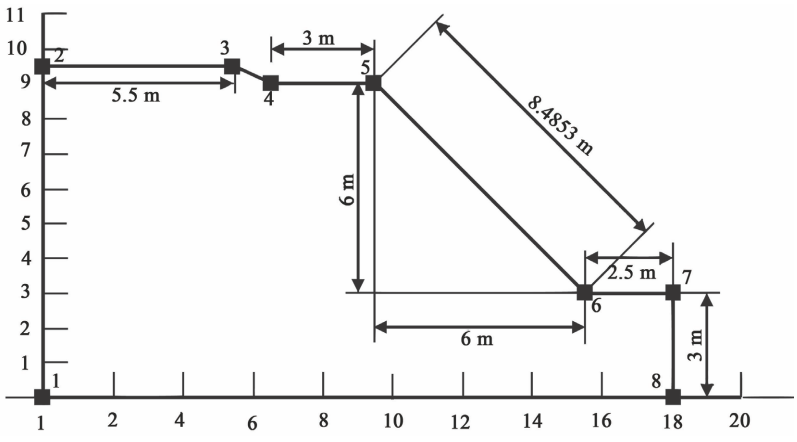

Figure 8. Model geometry.

During the surveys conducted in this section, no indications of water presence, such as a water table or springs, were identified. Nevertheless, in accordance with established geotechnical practices, precautions have been taken to prevent

unforeseen water ingress from the upper part of the massif and to mitigate rainwater infiltration.

Due to the very low seismic risk in Benin, seismic considerations will not be factored into the calculations.

2.3.2. Unreinforced Slope Stability

In this phase, we conduct calculations and perform an analysis to evaluate the stability of the slope without reinforcement, taking into account the mechanical properties of the soil layer.

a) Incorporating the layer into the software (**Figure 9**);

b) Incorporation of the sliding surface (**Figure 10**);

c) Deriving the safety factor using geotechnical data (**Figure 11**).

The stability analyses for the four limit equilibrium methods (Morgenstern-Price, Bishop, Janbu, Fellenius) conducted within SLOP/W are visualized in **Figure 8**. This figure highlights the critical failure plane associated with the minimum safety factor. Furthermore, a summary of the safety factor (Fs) values obtained using these four limit equilibrium methods is presented in **Table 7**.

2.4. Reinforced Slope Stability

After conducting simulations to assess the stability of the unreinforced slope, it became evident that the slope lacks stability. Therefore, reinforcement measures are imperative to ensure its long-term stability. The analysis of these reinforcements and their impact is discussed in the following sections.

2.4.1. Pile Reinforcement

During this phase, a single pile reinforcement is implemented in the upper portion of the unstable zone, perpendicular to the slope's direction. The piles used in this simulation are spaced three meters apart and possess a shear strength of 100 kN. The coordinates for these piles are provided in **Table 8**:

The results of the pile reinforcement on the slope and the positions of the piles are illustrated in **Figure 12**. It's worth noting that the safety coefficient obtained after the pile reinforcement of the slope is 2.034, indicating a substantial improvement compared to the initial state. Thus, it can be concluded that pile reinforcement effectively maintains or guarantees a certain level of slope stability.

2.4.2. Anchorage Reinforcement

In this phase, anchorage reinforcements are installed in the upper section of the unstable zone. The anchors used in this simulation have a shear strength of 100 kN and a pull-out strength of 200 kPa. Similar to the pile reinforcement, the anchors are spaced at three-meter intervals. The coordinates for the anchor locations are provided in **Table 8**. The results of the pile reinforcement on the slope and the positions of the piles are illustrated in **Figure 13**.

3. Results and Discussion

The results of this simulation reveal that the safety factors obtained through all

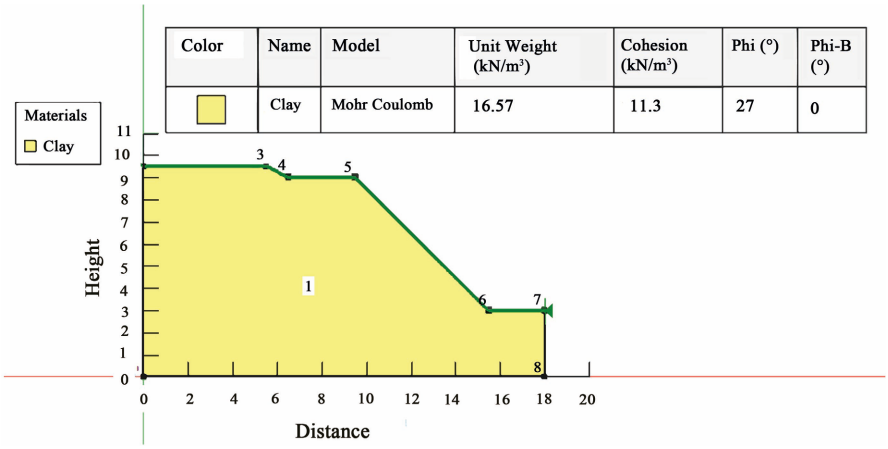

Figure 9. Inclusion of the layer and its associated geotechnical parameters into the software.

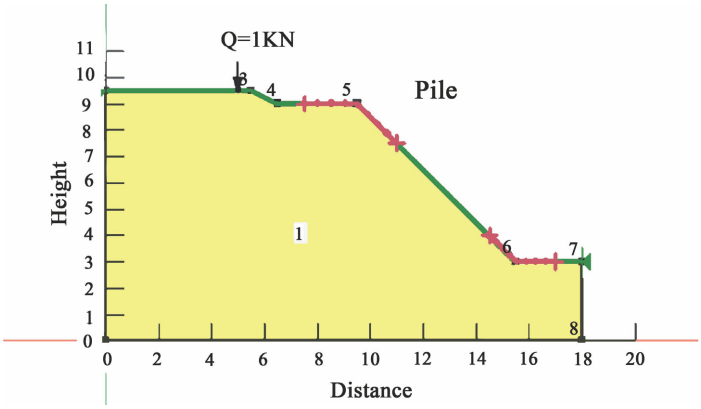

Figure 10. Inclusion of the sliding surface while accounting for applied overload.

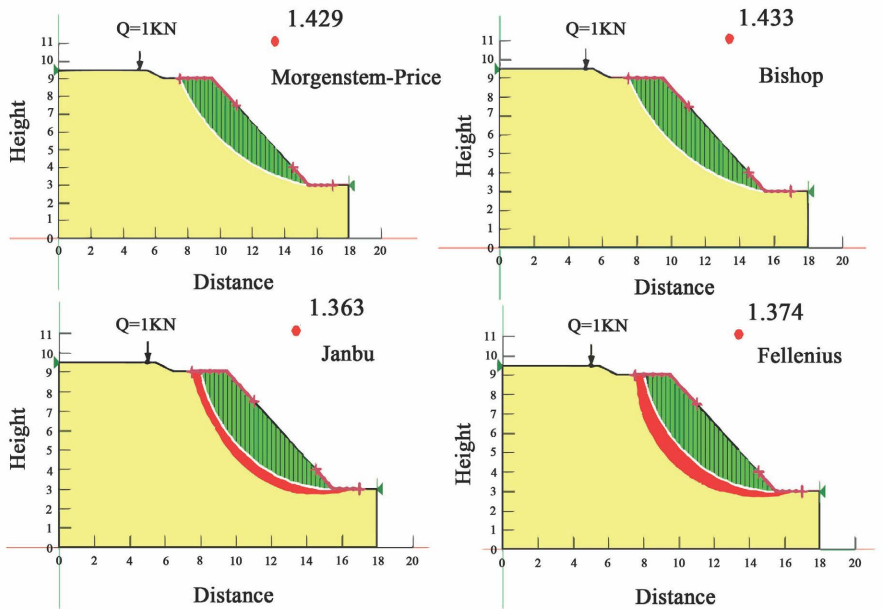

Figure 11. Fracture plane and Coefficient of Safety values for the four approaches.

Table 7. Factor of safety (Fs) using different methods.

Methods	Morgenstern-Price	Bishop	Janbu	Fellenius
Fs	1.429	1.433	1.363	1.374

Table 8. Piles and anchor reinforcement location.

Type of Reinforcement	Surface Coordinates (m)		Depth Coordinates (m)		Length (m)	Direction (˚)
	X	Y	X	Y		
Piles	12	6.5	12	2.5	4	90
Anchors	12	6.5	9.17	3.67	4	45

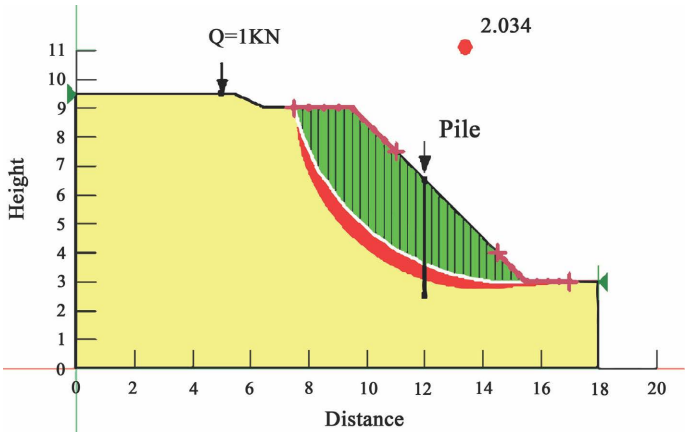

Figure 12. Pile reinforcement and corresponding safety factors.

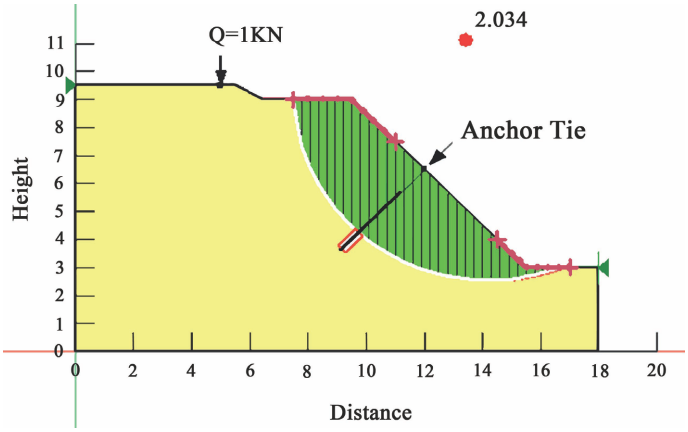

Figure 13. Anchor tie reinforcement and corresponding safety factors.

four methods are consistently below 1.5 (Fs < 1.5). As mentioned earlier, the Morgenstern-Price method is our preferred choice for calculations in this study. The safety factor obtained using this method indicates a critical state of the slope. Consequently, the embankment from KP1+750 to KP2+250 is currently assessed as unstable.

Among the considered methods, the Morgenstern-Price method emerges as

the one that adheres to all equilibrium conditions while providing the most accurate results. Therefore, for subsequent phases of embankment modeling, we have opted for the Morgenstern-Price method due to its ability to maintain equilibrium in both moment and force, making it the most precise analytical approach.

An additional comparison regarding the impact of cohesion (c) on the safety factor demonstrates a linear increase in the safety factor with higher cohesion values (Figure 14).

3.1. Anchors Parametric Study

We will conduct a parametric study by varying the angle of inclination with respect to the horizontal and evaluating its influence on the safety coefficient. Figure 15 illustrates how the safety coefficient changes in response to different anchor inclinations. When the anchor is inclined from 0˚ to 78˚ relative to the horizontal, the safety coefficient remains within the stable range. Remarkably, the most favorable condition is observed when the anchor is at 0˚ inclination from the horizontal.

Conversely, it's essential to note that safety coefficients fall below the stable zone when the anchor's inclination ranges from 80˚ to 360˚ downward.

In this phase, similar to the previous one, we maintain a friction angle of 0˚. However, we vary the shear force to assess its impact on the safety coefficient.

The safety coefficient curve as a function of the shear force reveals that, from an economic perspective, a shear force of 100 KN produces a more favorable safety coefficient. (Table 9)

In this phase, as in previous analyses, we favor an inclination angle of zero degrees (0˚). The friction angle remains fixed at 0˚, while we explore varying shear forces to observe their impact on the safety coefficient.

Figure 16 illustrates how the safety coefficient responds to changes in shear force. Remarkably, for practical and cost-effective considerations, a shear force of 100 KN delivers a more favorable safety coefficient.

At this stage, we also investigate the influence of altering the inclination angle concerning the horizontal axis and its subsequent effect on the safety coefficient.

3.2. Piles Parametric Study

Figure 17 depicts the variation in the safety coefficient concerning the pile's inclination angle. Within the range of 0˚ to 90˚ relative to the horizontal axis, the safety coefficient consistently resides within the stable zone. Moreover, the safety coefficient (Fs) curve exhibits a near-constant trend. Notably, reinforcing the pile with a 90˚ downward inclination from the horizontal proves most advantageous, ensuring both stability and practicality, as the safety coefficient (Fs) reaches 3.034.

Given the stability observed at the 90˚ angle, we maintain a fixed friction angle of 90˚ and proceed to analyze the safety coefficient's response to varying shear forces. Figure 18 presents the safety coefficient curve in relation to shear

Figure 14. Influence of cohesion on the safety factor.

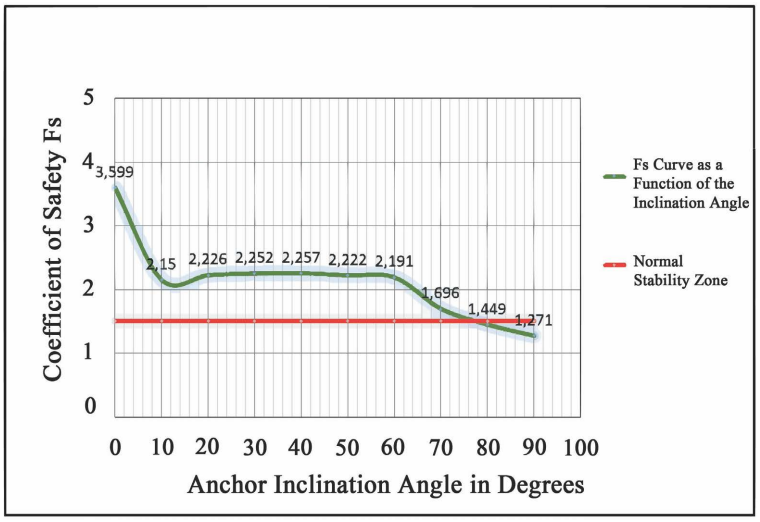

Figure 15. Safety factor vs. tie rod inclination angle.

Table 9. Safety factor (Fs) at different angles of inclination.

Angle of Inclination (˚)	Safety Factor (Fs)
0˚	3.599
10˚	2.150
20˚	2.226
30˚	2.252
40˚	2.257
50˚	2.222
60˚	2.191
70˚	1.696
80˚	1.449
90˚	1.271

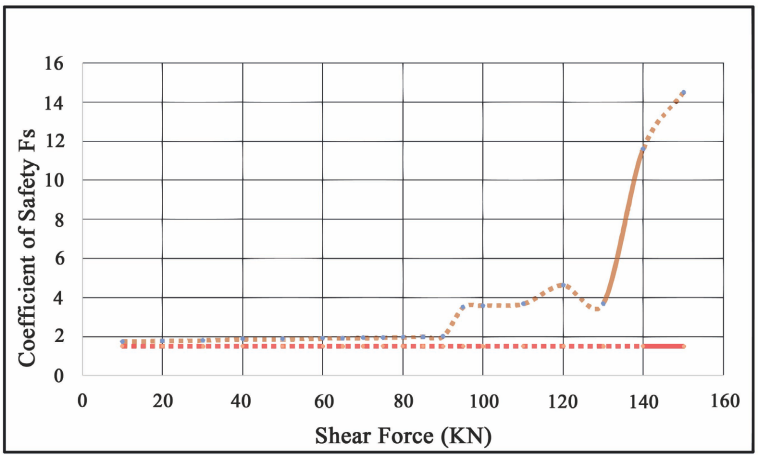

Figure 16. Curve of Fs vs. shear force.

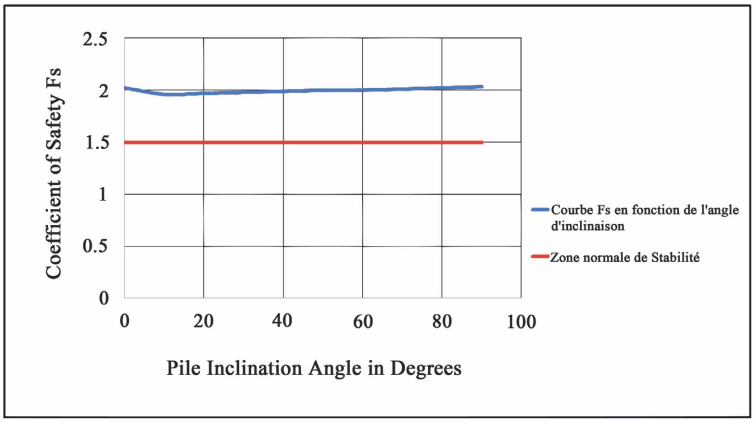

Figure 17. Safety factor variation based on pile inclination angle.

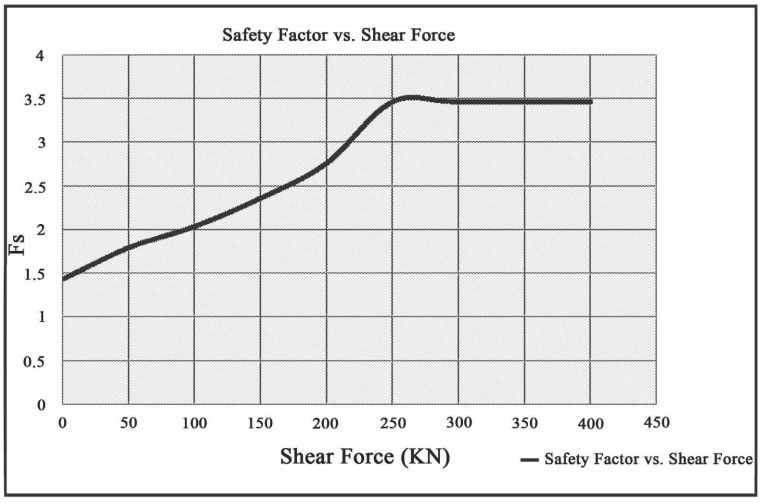

Figure 18. Safety factor vs. shear force.

force. It is evident that as shear force increases from 0 to 250 KN, the safety coefficient rises. Beyond 300 KN and onwards, the safety coefficient remains constant.

4. Conclusions and Suggestions

The study of slope failure occurrences along slopes relies on the utilization of safety factors. These factors can be defined as:

- The value by which the soil's resistance needs to be reduced (or gravity increased) for a failure to occur;
- The ratio between resisting forces (opposing failure) and driving forces.

The second definition, although more intuitive, is less prevalent in stability studies due to its higher complexity. Integrating a finite element method (FEM) with this definition presents an interesting alternative to SSRM or GIM.

In the context of the case study SLOP/W failure calculation methods are employed, encompassing Bishop, Janbu, Morgenstern-Price, and Fellenius techniques, grounded in principles of slice equilibrium, to conduct a numerical stability analysis of the embankment located between KP1+750 and KP2+250. Additionally, we delved into the influence of a pivotal parameter: cohesion. The outcomes of this stability assessment, executed with GEO-SLOP software, reveal that the present condition of the embankment is intrinsically unstable.

The SLOP/W calculations have unveiled potential hazards linked to slope instability. The modeling suggests that the principal contributors to this instability are the natural topography of the slope and the mechanical characteristics of the soil. To address these concerns and enhance stability, we explored two reinforcement techniques: pile reinforcement and anchor bolts. Both methods demonstrated substantial improvements in slope stability.

Acknowledgement

Authors gratefully acknowledge financial support for this work from the National Natural Science Foundation of China: Major Building and Bridge Structures and Earthquake Disaster Integration (91315301).

Data Availability Statement

Some or all data, models, or codes that support the findings of this study are available from the corresponding author upon reasonable request.

Conflicts of Interest

On behalf of all authors, the corresponding author states that there is no competing interest regarding the publication of this research.

References

[1] Boudlal, O. (2013) Etude expérimentale du comportement mécanique des fines dans la stabilité des talus et des foundations. Ph.D. Thesis, Université Mouloud Mammeri, Tizi-Ouzou.https://dspace.ummto.dz/items/cbc3ff5f-0381-47e9-9010-0aa82d23b1a1

[2] Benamara, F.Z. and Belabed, L. (2016) Analyse de la stabilité d'un talus routier renforcé par tirant d'ancrage par la méthode des éléments finis. *Academic Journal of Civil Engineering*, **34**, 481-487. https://doi.org/10.26168/ajce.34.1.59

[3] Guettouche, R. (2017) L'Analyse à priori de la stabilité au niveau de la carrière CHOUF AMMAR-M'SILA. Ph.D. Thesis, Ecole Nationale Supérieure des Mines et de la Métallurgie. Amar Laskri, Annaba.

[4] Djerbal, L. (2013) Analyse des mécanismes de déformation et de la rupture progressive du verssant instable d'Ain El Hammam. Ph.D. Thesis, Université Mouloud Mammeri, Tizi-Ouzou. https://dspace.ummto.dz/items/15144e04-ec6d-47d8-9c0c-313d6091002a

[5] Benaissa, A. and Bellouche, M.A. (1999) Propriétés géotechniques de quelques formations géologiques propices aux glissements de terrains dans l'agglomération de Constantine (Algérie) [Geotechnical Properties of Some Landslide-Prone Geological Formations in the Urban Area of Constantine (Algeria)]. *Bulletin of Engineering Geology and the Environment*, **57**, 301-310. https://doi.org/10.1007/s100640050049

[6] Belouar, A. (2005) Topologie, prévention du risque et cartographie géotechnique en site urbain-cas de la ville de Constantine. Master's Thesis, Université Mentouri Constantine, Constantine.

[7] Touitou, D, (2002) Apport de la modélisation et de l'instrumentation dans l'analyse de la stabilité et de la déformation à long terme d'un massif granitique: Application aux talus de grande hauteur de l'écluse à bateaux permanente au barrage des Trois Gorges (Chine). Master's Thesis, Ecole des Ponts ParisTech, Paris.

[8] Khebizi, M. (2006) Influence des glissements de terrain de la cité Boussouf (Constantine) sur les constructions. Master's Thesis, Université Mohamed Khider-Biskra, Biskra. http://thesis.univ-biskra.dz/id/eprint/1735

[9] Agbelele, K.J., Adeoti, G.O., Agossou, D.Y. and Aïsse, G.G. (2023) Study of Slope Stability Using the Bishop Slice Method: An Approach Combining Analytical and Numerical Analyses. *Open Journal of Applied Sciences*, **13**, 1446-1456. https://doi.org/10.4236/ojapps.2023.138115

[10] Agbelele, K.J., Houehanou, E.C., Ahlinhan, M.F., Aristide, H. C., *et al.* (2023) Assessment of Slope Stability by the Fellenius Slice Method: Analytical and Numerical Approach. *World Journal of Advanced Research and Reviews*, **18**, 1205-1214. https://doi.org/10.30574/wjarr.2023.18.2.0874

[11] Duncan, J.M. (1996) State of the Art: Limit Equilibrium and Finite-Element Analysis of Slopes. *Journal of Geotechnical Engineering*, **122**, 577-596. https://doi.org/10.1061/(ASCE)0733-9410(1996)122:7(577)

[12] Baker, R. (1980) Determination of the Critical Slip Surface in Slope Stability Computations. *International Journal for Numerical and Analytical Methods in Geomechanics*, **4**, 333-359. https://doi.org/10.1002/nag.1610040405

[13] Celestino, T.B. and Duncan, J.M. (1981) Simplified Search for Non-Circular Slip Surface. *Proceedings of the* 10*th International Conference on Soil Mechanics and Foundation Engineering*, Stockholm, 15-19 June 1981, 391-394.

[14] Greco, V.R. and Gulla, G. (1985) Slip Surface Search in Slope Stability Analysis. *Rivista Italiana di Geotecnica*, **19**, 189-198. https://associazionegeotecnica.it/wp-content/uploads/2010/09/RIG_1985_4_189.pdf

[15] Nguyen, V.U. (1985) Determination of Critical Slope Failure Surfaces. *Journal of Geotechnical Engineering*, **111**, 238-250. https://doi.org/10.1061/(ASCE)0733-9410(1985)111:2(238)

[16] Li, K.S. and White, W. (1987) Rapid Evaluation of the Critical Slip Surface in Slope Stability Problems. *International Journal for Numerical and Analytical Methods in Geomechanics*, **11**, 449-473. https://doi.org/10.1002/nag.1610110503

[17] Chen, Z.Y. (1992) Random Trials Used in Determining Global Minimum Factors of

Safety of Slopes. *Canadian Geotechnical Journal*, **29**, 225-233. https://doi.org/10.1139/t92-026

[18] Greco, V.R. (1987) Efficient Monte Carlo Technique for Locating Critical Slip Surface. *Journal of Geotechnical Engineering*, **122**, 517-525. https://doi.org/10.1061/(ASCE)0733-9410(1996)122:7(517)

[19] Malkawi, A.I.H., Hassan, W.F. and Sarma, S.K. (2001) Global Search Method for Locating General Slip Surface Using Monte Carlo Techniques. *Journal of Geotechnical and Geoenvironmental Engineering*, **127**, 688-698. https://doi.org/10.1061/(ASCE)1090-0241(2001)127:8(688)

[20] Cheng, Y.M. (2003) Location of Critical Failure Surface and Some Further Studies on Slope Stability Analysis. *Computers and Geotechnics*, **30**, 255-267. https://doi.org/10.1016/S0266-352X(03)00012-0

[21] Fellenius, W. (1927) Erdstatische Berechnungen mit Reibung und Kohäsion (Adhäsion) und unter Annahme kreiszylindrischer Gleitflächen. W. Ernst & Sohn, Hoboken.

[22] Bishop, A.W. (1955) The Use of the Slip Circle in the Stability Analysis of Slopes. *Geotechnique*, **5**, 7-17. https://doi.org/10.1680/geot.1955.5.1.7

[23] Lowe, J. and Karafiath, L. (1960) Stability of Earth Dams upon Drawdown. https://cir.nii.ac.jp/crid/1571980074835346688

[24] US Army Corps of Engineers (1970) Stability of Earth and Rock-Fill Dams. United States Army Engineer Waterways Experiment Station, Vicksburg.

[25] Morgenstern, N.R. and Price, V.E. (1965) The Analysis of the Stability of General Slip Surfaces. *Geotechnique*, **15**, 79-93. https://doi.org/10.1680/geot.1965.15.1.79

[26] Spencer, E. (1967) A Method of Analysis of the Stability of Embankments Assuming Parallel Inter-Slice Forces. *Geotechnique*, **17**, 11-26. https://doi.org/10.1680/geot.1967.17.1.11

[27] Janbu, N. (1968) Slope Stability Computations, Soil Mechanics and Foundation Engineering Report. Technical University of Norway, Trondheim.

[28] Duncan, J.M., Buchignani, A.L. and DeWet, M. (1987) An Engineering Manual for Slope Stability Studies. Department of Civil Engineering, Geotechnical Engineering, Virginia Polytechnic Institute and State University, Blacksburg.

[29] Alexis, A. (1987) Etude geotechnique et sedimentologique de souilles et chenaux de la rade de lorient: Contribution a la stabilite des sols immerges. https://www.theses.fr/1987NANT2033

[30] M'zoughem, K. and Chenafa, W. (2006) Etude géotechnique de la stabilité des talus dans la carrière de Ain El Kebira (Setif). Master's Thesis, University of Ferhat Abbas, Setif.

[31] Haoues, N. and Loucif, S. (2017) Etude de stabilité d'une Talus. Real Case: Ciloc-Constantine City. Master's Thesis, Larbi Ben M'hidi University of Oum El Bouaghi, Oum El Bouaghi. http://bib.univ-oeb.dz:8080/jspui/bitstream/123456789/7438/1/HAOUES%20NASSIMA-LOUCIF%20SARA.pdf